EasyChair Preprint

№ 2017

Advantages of Charge Plasma Based Double Gate Junction-less MOSFET over Bulk MOSFET for Label Free Biosensing

Amit Bhattacharyya, Adrija Mukherjee, Manash Chanda and Debashis De

November 21, 2019

Advantages of Charge Plasma Based Double Gate Junction-less MOSFET over Bulk MOSFET for Label Free Biosensing

Amit Bhattacharyya
Electronics and Communication Engineering Dept.
Haldia Institute of Technology
Haldia, India
amit_elec06@yahoo.com

Adrija Mukherjee
Electronics and Communication Engineering Dept.
Meghnad Saha Institute of Technology
Kolkata, India
adrijamukherjee06@gmail.com

Manash Chanda
Member, IEEE,
Electronics and Communication Engineering Dept.
Meghnad Saha Institute of Technology
Kolkata, India
manash.chanda.1983@ieee.org

Debashis De
Senior Member, IEEE,
Computer Science and Engineering Dept.
Maulana Abul Kalam Azad University of Technology
Kolkata, India
dr.debashis.de @ieee.org

ABSTRACT

An assessment of charge plasma (CP) based biosensing between junction less (JL) and conventional devices for label-free electrical identification of analytes, especially DNA, has been examined here in detail. The impact of variations of charge analytes immobilized inside the nanogap cavity over the drain current, energy band profile, electron concentration, and sensitivity evaluated in dry atmospheric conditions. Here, the shifts into threshold potential for both JL-MOSFET and conventional-MOSFET based biosensor architecture have been utilized, like the sensing factor, to identify the existence of analytes while they immobilized inside the nanogap cavity in the channel section. The design of the recommended model with the complete numerical analysis has been executed utilizing the ATLAS device simulation software.

Keywords: Biosensor, Electron concentration, Flat-band voltage, Junctionless metal oxide semiconductor field effect transistor (MOSFET), Sensitivity, Threshold voltage, Work-function.

I. INTRODUCTION

With the commencement of Ion-sensitive field-effect transistors (ISFET) in 1970 by Bergveld [1], ISFET and it's imitative admire for electrical identification of charged biospecies. Still, it had severe restrictions, akin to low recognition ability of neutral bioanalytes, as well as inappropriateness by the typical complementary metal-oxide-semiconductor (CMOS) skill [2]. Subsequently, the perception of dielectric modulated FET (DMFET) was projected [3], having a nanogap cavity allowing label-free identification of both charged as well as neutral biospecies also with high sensitivity. Furthermore, dry atmospheric situations have chosen, which may offer an elevated degree of freedom for different configurations that can progress sensors' features [4] in various fields like medical study [5], food inspection [6], and crime detection [7] etc.

Jin *et al.* [8] and Lee *et al.* [9], in their work, pointed out the benefits of junctionless (JL) MOSFET above conventional Inversion-mode (IM) MOSFET for providing low gate leakage current, low drain induced barrier lowering (DIBL), enhanced ON/OFF current fraction (I_{ON}/I_{OFF}) as well as simple fabrication process due to uniform doping concentration throughout source, drain and channel region. Long *et al.* [10] have demonstrated that dual material gate (DMG) structure can improve carrier transfer competence, transconductance (which was distressed by JL structure), short channel effects (SCEs) as well as drain output resistance above single material gate (SMG) arrangement [11]. Furthermore, the juxtaposition of low-k Silicon dioxide (SiO2) and high-k dielectric material (namely, TaO2, TiO2, HfO2, etc.), is preferred as gate oxide to improve carrier mobility and hence gets better device transconductance, ON current, reduction of gate leakage current, etc [12]. The disadvantage of positional supported sensitivity in tunnel FET (TFET) may be surmounted via Junctionless MOSFET based biosensing configuration as this is exempt from ambipolar consequence [13], as well as further significantly, the conduction method takes place via drift-diffusion of the carriers over the barrier.

In this paper, a CP-based device configuration has recommended with design after combining the benefits of JL-MOSFET configuration, DMG, and DG architectures, and low-k/high-k oxide stack for gate insulator, called charge plasma-based dual metal double gate with oxide stack junctionless MOSFET (CP-DM-DG-OS JL-MOSFET), to use it as biosensing arrangement for label-free electrical recognition of bioanalytics, especially DNA utilizing dielectric modulation (DM) scheme. Moreover, a nanogap is formed within the high-k dielectric of gate stack to incorporate the biospecies in the cavity, placed either at drain end or source end. A one-to-one comparison of the performance of such a circuit made with that built with conventional MOSFET. The impact of

variations of charge of bioanalytics over the drain current, energy band profile, electron concentration, and sensitivity for both JL-MOSFET and conventional MOSFET has scrutinized.

This article is organized likely follows: Section II illustrates the device configuration along with their dimensions and parameters and simulation setup with the calibrated model. Section-III deals with the results of numerical analysis of the proposed CP-DM-DG-OS JL-MOSFET, and finally, in section-IV, the significant-conclusion about our work has been drawn.

II. STRUCTURAL DESCRIPTIONS WITH SIMULATION APPROACH

A schematic of n-type Silicon made charge plasma-based dual metal double gate with oxide stack junctionless MOSFET (CP-DM-DG-OS JL-MOSFET), applicable in this work as biosensor, illustrated in Fig. 1. Intended for the bioanalyte hybridization, nanogap cavity having cavity length (L_{cavity}) = 400 nm and cavity height (T_{cavity}) = 10 nm created inside JL MOSFET via engraving some portion of high-k material, sandwiched between gate metal and low-k oxide film from source and drain portion of channel once at a time as depicted in Fig. 1(a) and (b). Both the device configuration consists of uniformly doped ($1\times10^{15}/cm^3$) source, drain and channel region having gate oxide stack consisting of a 1-nm-thick low dielectric constant [SiO_2 (k = 3.9)] bottom layer (T_{oxl}) and a 10-nm-thick high-k [HfO_2 (k = 22)] top layer (T_{oxh}), after Swain *et al.*[14]. Channel length (L_{ch}) =1µm, channel thickness (T_{si}) = 8 nm, equal-sized source and drain regions ($L_S = L_D$ = 10 nm) are chosen for our work. For the concept of dual metal [15], the gate electrode region has been divided equally into two parts, namely gate metal M_1 (length L_1 = 500 nm) close to the source end and gate metal M_2 close to the drain end (length L_2 = 500 nm). A thin layer of aluminum considered as a drain and source electrode. Titanium (work-function, ϕ_M = 4.33 eV) and Gold (ϕ_M = 5.3 eV) have been selected as gate metals [16]. In our work, we have described the impact of the relative positioning of gate metals on electrical characteristics of JL-MOSFET and conventional MOSFET to examine its sensitivity. A layer of low-k SiO_2, isolating cavity from silicon body, protects gate-to-channel outflow and besides acts as a bonding coat to hybridize the bioanalytes in the cavity region. In practice, a well-designed surface of the cavity region is a must to immobilize the biomolecules. The target biospecies can be identified after the formation of sensing sites in the nanogap cavity regions.

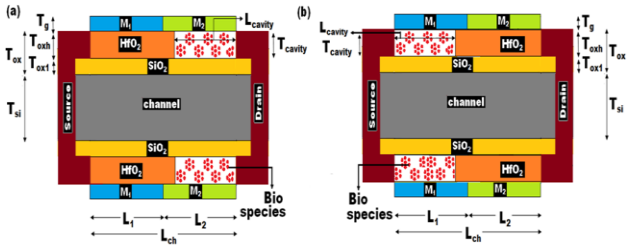

Fig. 1. Schematic of CP-DM-DG-OS JL-MOSFET with nanogap cavity (a) placed at drain part of the channel section (b) placed at source part of the channel section.

Simulations of CP-DM-DG-OS JL-MOSFET and conventional MOSFET based biosensor structures and to study their electrical characteristics, a commercially available numerical simulator, Silvaco ATLAS, version 5.18.3.R [17] has been utilized. All the horizontal contours are recognized at a distance of 0.5 nm from the oxide-semiconductor interface. Boltzmann transport equation (BTE), band-gap narrowing (BGN), Shockley Read Hall (SRH) recombination and generation for concentration-dependent carrier lifetime, concentration-dependent mobility model, quantum density gradient form to consider quantum-mechanical consequences, the Fermi-Dirac carrier distribution models have been utilized to simulate the electrostatics as well as current. The models with methods used for simulation are well-calibrated with experimental consequences of Duarte *et al.* [18] as exposed in Fig. 2. We have chosen the same parameters and their values, as used by Duarte *et al.* [18] to develop their analytical model. Good agreement of the simulation, as well as practical results for the device structure, is evident in Fig. 2.

Charged analytes consist of charge as well as dielectric constant as well, e.g. non-hybridized single-strand DNA has the possessions of charge and dielectric constant too [19]. As a consequence, the existence of charged bioanalytes inside the nanogap cavity region is presented into our simulation via introducing settled oxide charges ($N_f = \pm\ 5\times10^{15}/m^2$) at some suitable position within the gate insulator itself. In the present circumstances, for JL-MOSFET and Conventional MOSFET based biosensor applications, the longer length of the channel of the device structure is favored, as the facility of proper binding of a good many numbers of bioanalytes with the sensing surface is relatively weak at the nanoscale regime [20]. Due to this reason, throughout our simulation work, we have utilized a 1-µm channel length JL-MOSFET and conventional MOSFET; even though for superior device performances, the shorter channel length is compulsory. In this paper, we have considered standard dielectric constant of neutral protein biomolecules, especially enzymes, e.g., Apomyoglobin having dielectric constant, k=8, and radius is 20 Å [21].

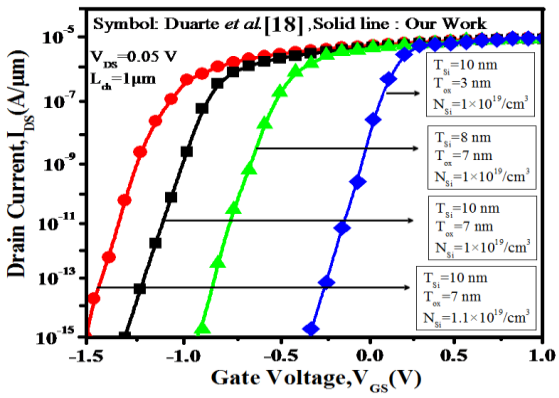

Fig. 2. Model calibration of our simulated I_{DS}-V_{GS} curves for CP-DM-DG-OS JL-MOSFET with those of Duarte *et al.*s' analytical work [18] at V_{DS} = 50 mV, Source/drain length, L_S/L_D=10 nm.

III. RESULTS AND DISCUSSIONS

A. Effect of charged analytes over drain current of longer channel length CP-DM-DG-OS JL-MOSFET and conventional MOSFET

Here, the spotlight of our discussion is on the transistor characteristics which are found to be sensitive with the variation of potential about the channel for the existence of charged biospecies. Fig. 3(a)-(d) and Fig. 4(a)-(d) show the relative shift in transfer characteristics of JL-MOSFET and conventional MOSFET based biosensor due to effective variation in gate charge after immobilization of different charged biomolecules within the nanogap cavity, irrespective of their position in the channel region and after swapping the positions of two gate metals, for both source and drain end cavity. The figure reveals that the I_{OFF} reduces for negatively charged analytes ($-5\times10^{15}/m^2$), whereas the same for positively charged analytes ($+5\times10^{15}/m^2$) increases, in comparison with that corresponding to the neutral analytes (here, apomyoglobin with k = 8).

This is mainly due to the variation in semiconductor surface potential, being influenced by the variation in flat-band voltage which in fact depends upon the charge of analytes exists in the cavity following the relation,

$$\Delta V_{fb} = \frac{qN_f}{C_{eff}} \qquad (1)$$

Thus, by an enhancement of negatively charged bioanalytes in the cavity, source-channel barrier height enhances, which results in a reduction of drain current; but just the reverse things happen with the positive charge in the cavity. Furthermore, as the concentration of the doping level inside the channel section of conventional MOSFET is less (is of the order of $10^{17}/cm^3$) than that of JL-MOSFET structure, hence the drain current going to be reduced as depicted in the Fig. 4(a)-(d).

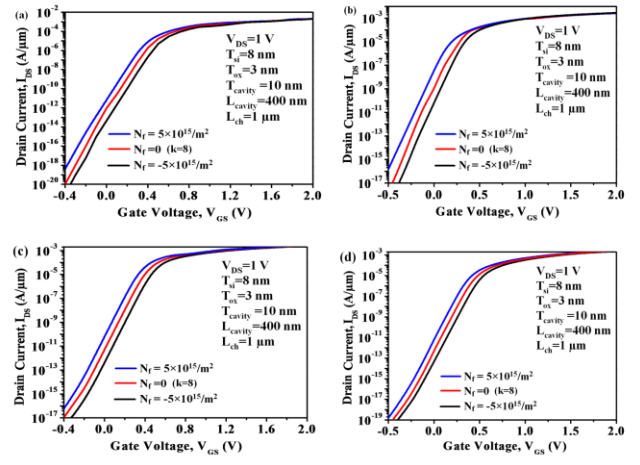

Fig. 3. Characteristics of I_{DS}-V_{GS} for CP-DM-DG-OS JL-MOSFET with charged biomolecules present at (a) drain end cavity for $\phi_{M1} > \phi_{M2}$ (b) source end cavity for $\phi_{M1} > \phi_{M2}$ (c) drain end cavity for $\phi_{M2} > \phi_{M1}$ (d) source end cavity for $\phi_{M2} > \phi_{M1}$ at V_{DS} = 1V, L_{ch}=1μm

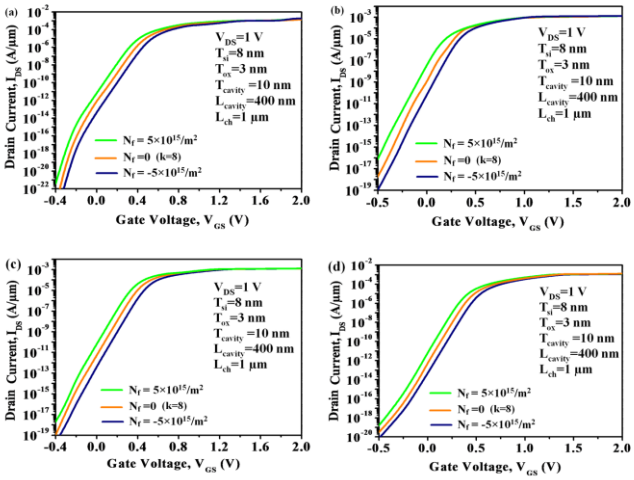

Fig. 4. Characteristics of I_{DS}-V_{GS} for conventional MOSFET with charged biomolecules present at (a) drain end cavity for $\phi_{M1} > \phi_{M2}$ (b) source end cavity for $\phi_{M1} > \phi_{M2}$ (c) drain end cavity for $\phi_{M2} > \phi_{M1}$ (d) source end cavity for $\phi_{M2} > \phi_{M1}$ at V_{DS} = 1V, L_{ch}=1μm

B. Influence of charged analytes over energy band and electron concentration profiles of longer channel length CP-DM-DG-OS JL-MOSFET and conventional MOSFET

Here, we focus on the energy-band contour with the corresponding concentration profile of electrons along the length of the channel of CP-DM-DG-OS JL-MOSFET based device, after the immobilization of charged biospecies inside the cavity. Fig. 5(a) and (b) illustrate the influence of charged biospecies over energy band profiles of the JL-MOSFET based device with a cavity placed at drain end and source end, respectively, for $V_{DS} \sim 0$ V and $V_{GS} = -0.5$ V, keeping $\phi_{M1} > \phi_{M2}$. When $\phi_{M1} > \phi_{M2}$, a high electric field, exists on the semiconductor surface (through gate-oxide stack) mainly under the portion of

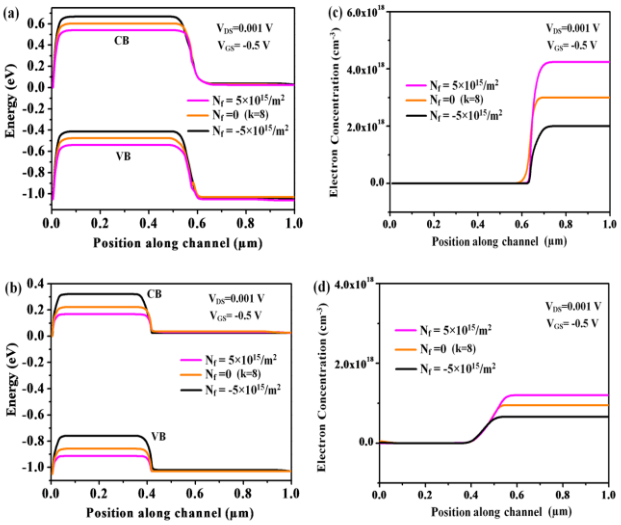

Fig. 5. Energy band diagrams [(a) & (b)] and electron concentration profiles [(c) & (d)] with charged biomolecules, respectively, at drain end cavity and at source end cavity for $\phi_{M1} > \phi_{M2}$, corresponding to V_{DS} = 0.001V and V_{GS} = -0.5V, of CP-DM-DG-OS JL-MOSFET having L_{ch}=1μm.

high work-function metal gate drives the electrons to get depleted from the source side of the channel region, and hence, electron concentration reduces there. Correspondingly, due to devoid of free electrons (manifested as a very high resistive zone), energy bands of the regime, bend up relative to the energies of other parts of semiconductor surrounding to that region in question, and thus source-to-channel barrier height increases. Theoretically, any change in electrostatic potential due to the inclusion/exclusion of charged biospecies in the nanogap cavity, whether placed on drain portion or source portion, is mostly absorbed in that high resistive zone located at the source side of the channel, leading to modulation of source-to-channel barrier height only. So, negatively charged biospecies (– 5×1015/m2), conjugated within the cavity region, help move the semiconductor conduction and valence bands even upward, whereas the same for positively charged biospecies (+5×1015/m2) are pushed downward in comparison with those corresponding to the neutral biospecies (for apomyoglobin with k = 8). Depending on the heights of the barrier number of electrons, surmounting them changes as well. Still, they cannot reside within the high electric-field (depletion) zone of the semiconductor. Rather it favors them electrostatically to get piled up towards the drain end of the channel, considered as deficient field regime under the portion of the gate having low work-function metal as an electrode, and, therefore, electron concentration only changes there, as may be evidenced as of Fig. 5(c) and (d). Similar kinds of contours can also be found, as already verified by us, for the device with either a source or a drain end cavity, keeping $\phi_{M2} > \phi_{M1}$ as shown in Fig. 6(a)-(d).

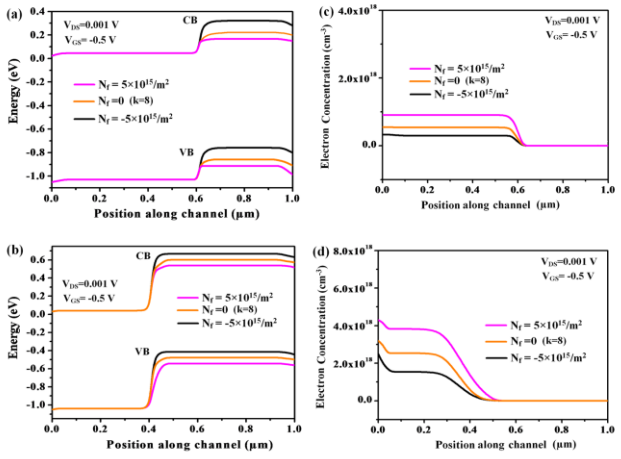

Fig. 6. Energy band diagrams [(a) & (b)] and electron concentration profiles [(c) & (d)] with charged biomolecules, respectively, at drain end cavity and at source end cavity for $\phi_{M2}>\phi_{M1}$, corresponding to V_{DS} = 0.001V and V_{GS} = -0.5V, of CP-DM-DG-OS JL-MOSFET having L_{ch}=1μm

Similar nature of energy band diagram and the corresponding electron concentration profile along the length of the channel of conventional MOSFET based device, after the immobilization of charged biospecies inside the nanogap cavity can also be found, as already verified by us, with either a source or a drain end cavity, keeping $\phi_{M1} > \phi_{M2}$ and $\phi_{M2} > \phi_{M1}$ as exposed in Fig. 7(a) - 7(d) and 8(a) - (d) correspondingly. Since the concentration of the doping level inside the channel section of conventional MOSFET is less (is of the order of $10^{17}/cm^3$) than that of JL-MOSFET structure, the electron concentration in that region becomes less and hence the drain current going to reduce. Consequently, the source-to-channel barrier height of conventional MOSFET increases than that of JL-MOSFET structure, as shown in Fig. 7(a)-(d) and 8(a)-(d).

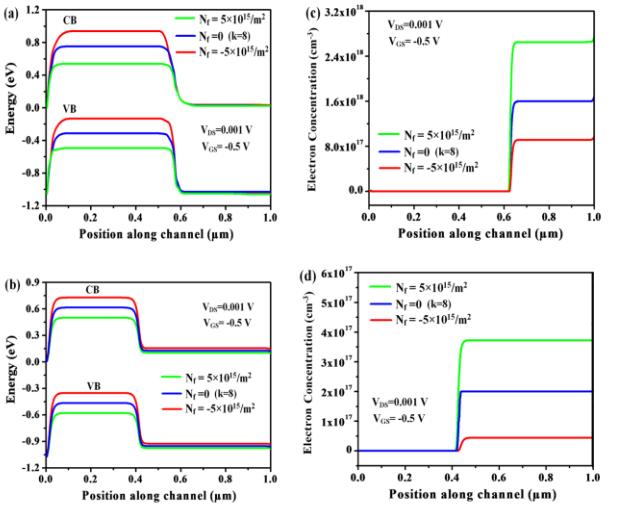

Fig. 7. Energy band diagrams [(a) & (b)] and electron concentration profiles [(c) & (d)] with charged biomolecules, respectively, at drain end cavity and at source end cavity for $\phi_{M1}>\phi_{M2}$, corresponding to V_{DS} = 0.001V and V_{GS} = -0.5V, of conventional MOSFET having L_{ch}=1μm.

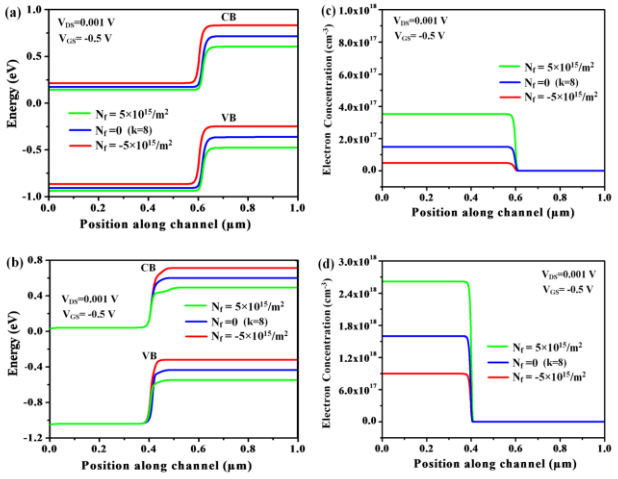

Fig. 8. Energy band diagrams [(a) & (b)] and electron concentration profiles [(c) & (d)] with charged biomolecules, respectively, at drain end cavity and at source end cavity for $\phi_{M2}>\phi_{M1}$, corresponding to V_{DS} = 0.001V and V_{GS} = -0.5V, of conventional MOSFET having L_{ch}=1μm.

In this paper, we have chosen threshold voltage (V_{th}) as a figure-of-merit to study the sensitivity of both CP-DM-DG-OS JL-MOSFET based biosensor and conventional MOSFET based biosensor, since after interaction between biospecies and sensing sites of the cavity region generally its values get altered significantly.

The sensitivity for charged analytes can be expressed by some mathematical formulae, as follows:

$$\Delta V_{th} = \left| V_{th}(N_f = 0) - V_{th}(Ch\arg ed) \right|; \quad (2)$$

$$S_{CBio} = \left| \frac{V_{th}(N_f) - V_{th}(ch\arg ed)}{V_{th}(N_f)} \right|; \quad (3)$$

Fig. 9(a)-(d) illustrates the impact on sensitivity parameter, ΔV_{th} when charged biospecies are immobilized within the cavity, irrespective of their position in the channel region and after swapping the positions of two gate metals, for both source and drain end cavity. Figures reveal that the sensitivity factor, ΔV_{th}, directly enhances with the increase of charge of the biomolecules commenced inside the cavity. This has also observed that the sensitivity factor, ΔV_{th} of both CP-DM-DG-OS JL-MOSFET and conventional MOSFET based biosensor is more influenced by the negatively charged biospecies.

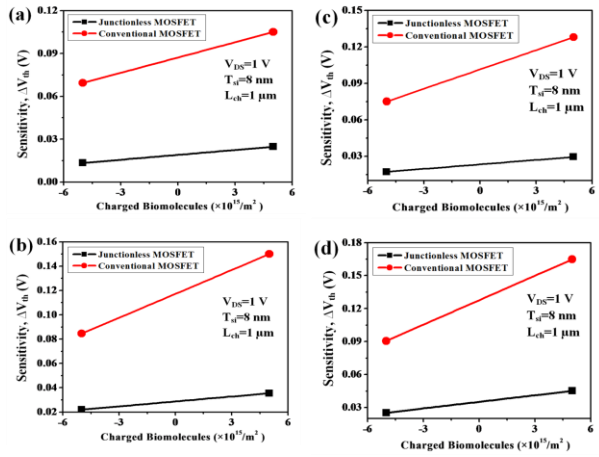

Fig. 9. Variation of sensitivity parameter, ΔV_{th} for both CP-DM-DG-OS JL-MOSFET and conventional MOSFET based biosensor in presence of charged biomolecules at (a) drain end cavity for $\phi_{M1} > \phi_{M2}$ (b) source end cavity for $\phi_{M1} > \phi_{M2}$ (c) drain end cavity for $\phi_{M2} > \phi_{M1}$ (d) source end cavity for $\phi_{M2} > \phi_{M1}$ at V_{DS} = 1V, L_{ch}=1µm.

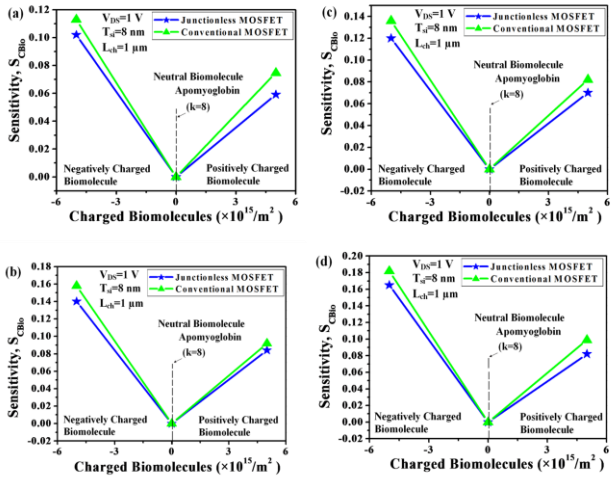

Fig. 10. Variation of sensitivity parameter, S_{CBio} for both CP-DM-DG-OS JL-MOSFET and conventional MOSFET based biosensor in presence of charged biomolecules at (a) drain end cavity for $\phi_{M1} > \phi_{M2}$ (b) source end cavity for $\phi_{M1} > \phi_{M2}$ (c) drain end cavity for $\phi_{M2} > \phi_{M1}$ (d) source end cavity for $\phi_{M2} > \phi_{M1}$ at V_{DS} = 1V, L_{ch}=1µm.

The influence of charged biospecies over the sensitivity parameter, S_{CBio}, is represented in Fig. 10(a)-(d) for both CP-DM-DG-OS JL-MOSFET and conventional MOSFET based biosensor, irrespective of the cavity position in the channel region and after swapping the positions of two gate metals, for both source and drain end cavity. As evidenced by Fig. 10(a)-(d), it might be claimed that the sensitivity factor, S_{CBio} of both CP-DM-DG-OS JL-MOSFET and conventional MOSFET based biosensor, is more influenced by the negatively charged biospecies.

IV. CONCLUSION

Comparative performance analysis of JL-FET and conventional FET based biosensor is presented. The transduction mechanism, in either case, is based on the conjugation of charged or neutral biomolecules in the cavity. In either device, the performance is evaluated in terms of conjugation induced modulation in drain current and shift in threshold voltage by configuring the cavity near the drain-channel and source-channel junction at a time. The simulation results reveal that the sensitivity parameters, ΔV_{th} and S_{CBio} for both the devices, are further persuaded via the negatively charged bioanalytes independent of the position of high work-function gate metal and irrespective of the cavity position in the channel region. The sensitivity parameter, ΔV_{th} of conventional FET is compared with the JL-FET based biosensor structure, and a 119.6 mv (65.4 mv) improvement is observed for the existence of negatively (positively) charged analytes inside the cavity since the channel doping concentration of conventional FET is relatively lower than that of JL-FET as represented in Fig. 9(a). A more or less similar trend of variation of ΔV_{th} can be observed for Fig. 9(b)-(d). Fig. 10(a) depicts that an improvement of sensitivity parameter, S_{CBio} by an amount of 0.007(0.0028), is obtained for the existence of negatively (positively) charged analytes in the nanogap cavity of conventional FET based biosensor structure when compared with JL-FET. A more or less similar trend of variation of S_{CBio} can also be observed for Fig. 10(b)-(d). Thus, Conventional FET based biosensor offers better sensitivity than JL-FET based biosensor.

REFERENCES

[1] P. Bergveld, "Development of an ion-sensitive solid-state device for neuro physiological measurements," *IEEE Trans. Biomed. Eng.*, vol. 17, no. 1, pp.70–71, Jan. 1970.

[2] Y. Cui, Q. Wei, H. Park, and C.M. Lieber, "Nanowire nanosensors for highly sensitive and selective detection of biological and chemical species," *Science*, vol. 293, no. 5533, pp.1289–1292, Aug. 2001.

[3] H. Im, X.-J. Huang, B. Gu, and Y.-K. Choi, "A dielectric-modulated field effect transistor for biosensing," *Nat. Nanotechnol.*, vol. 2, no. 7, pp. 430–434, Jul. 2007.

[4] J. Y. Kim, J. H. Ahn, S. J. Choi, M. Im, S. Kim, J. P. Duarte, C. H. Kim, T. J. Park, S. Y. Lee, and Y. K. Choi, "An underlap channel-embedded field-effect transistor for biosensor application in watery and dry environment, *IEEE Trans. Nanotechnol.*, vol. 11, no. 2, pp. 390–394, March 2012.

[5] C. Ribaut *et al.*, "Cancer biomarker sensing using packaged plasmonic optical fiber gratings: Towards in vivo diagnosis," *Biosensors Bioelectron.*, vol. 92, pp. 449–456, Jun. 2017.

[6] M. Sheikhshoaie, H. Karimi-Maleh, I. Sheikhshoaie, and M. Ranjbar,"Voltammetric amplified sensor employing RuO2 nano-road and room temperature ionic liquid for amaranth analysis in food samples," *J. Mol. Liq.*, vol. 229, pp. 489–494, Mar. 2017.

[7] J. Shin, S. Choi, J.-S. Yang, J. Song, J.-S. Choi, and H.-I. Jung, "Smart forensic phone: Colorimetric analysis of a bloodstain for age estimation using a smartphone," *Sens. Actuators B, Chem.*, vol. 243, pp. 221–225, May 2017.

[8] X. Jin, X. Liu, M. Wu, R. Chuai, J.-H. Lee, and J.-H. Lee, "A unified analytical continuous current model applicable to accumulation mode (junctionless) and inversion mode MOSFETs with symmetric and asymmetric double-gate structures," *Solid- State Electron.*, vol. 79, pp. 206–209, Jan. 2013.

[9] C. W. Lee *et al.*, "High-temperature performance of silicon junctionless MOSFETs," *IEEE Trans. Electron Devices*, vol. 57, no. 3, pp. 620-625, Mar.2010.

[10] W. Long, H. Ou, J.-M. Kuo, and K. K. Chin, "Dual-material gate (DMG) field effect transistor," *IEEE Trans. Electron Devices*, vol. 46, no. 5, pp. 865–870, May 1999.

[11] H. Lou, L. Zhang, Y. Zhu, X. Lin, S. Yang, and J. He, *et al.*, "A junctionless nanowire transistor with a dual-material gate," *IEEE Trans. Electron Devices*, vol. 59, no. 7, pp. 1829–1836, Jul. 2012.

[12] F. Djeffal, Z. Ghoggali, and Z. Dibi, et al., " Analytical analysis of nanoscale multiple gate MOSFETs including effects of hot -carrier induced interface charge," *Microelectron. Reliab.* Vol. 49, no. 4, pp. 377–381, Apr. 2009.

[13] R. Narang, M. Saxena, and M. Gupta, "Comparative analysis of dielectric-modulated FET and TFET-based biosensor," *IEEE Trans. Nanotechnol.*, vol. 14, no. 3, pp. 427–435, 2015.

[14] S.K. Swain, A. Dutta, S. Adak, and C.K. Sarkar, " Influence of channel length and high-K oxide thickness on subthreshold analog/RF performance of graded channel and gate stack DG-MOSFETs," *Microelectron. Reliab.* Vol. 61, pp. 24-29, Mar. 2016.

[15] R. K. Baruah, and R. P. Paily, "A dual–material gate junctionless transistor with high-k spacer for enhanced analog performance," *IEEE Trans. Electron Devices*, vol. 61, no. 1, pp. 123–128, Jan. 2014.

[16] W. M. H. Sachtler, G. J. H. Dorgelo, and A. A. Holscher, "The work function of gold," *Surface Science*, vol. 5, no. 2, pp. 221-229, Oct.1966.

[17] ATLAS Device Simulation Software, Silvaco Int., Santa Clara, CA, USA, 2015.

[18] J. P. Duarte, S. J. Choi, D. T. Moon, and Y. K. Choi, "Simple analytical bulk current model for long-channel double –gate junctionless transistors," *IEEE Electron Device Lett.*, vol. 32, no. 6, pp. 704–706, Jun. 2011.

[19] C. H. Kim, C. Jung, and Y.K. Choi, "Novel dielectric modulated field-effect transistor for label-free DNA detection," Biochip J., vol. 2, no. 2, pp. 127-134, Jun. 2008.

[20] H. Im, X. J. Huang, B. Gu, and Y.K. Choi, "A dielectric modulated field-effect transistor for biosensing," Nat. Nanotechnol. vol. 2, no. 7, pp. 430–434, Jun. 2007.

[21] T. Simonson and C. L. Brooks, "Charge screening and the dielectric constant of proteins: insight from molecular dynamics," *J. Am. Chem. Soc.* vol. 118, no. 35, pp. 8452–8458, Sep. 1996.